Supplementary Information

3D-Printed Liquid Handling Robot for the Development of Automated Analytical Methods

Aline D. Assunção,[#,a] Diogo M. de Jesus,[#,a] Teodoro R. Terra,[a] Raquel G. Rocha,[a] José A. M. G. Costa,[a] Luiz A. J. da Silva,[a] Guilherme L. Fernandes,[b] Alessandro G. C. Dias,[b] Rodrigo A. A. Muñoz,[a] Sidnei G. Silva[a] and Eduardo M. Richter[,a]*

[a]*Instituto de Química, Universidade Federal de Uberlândia, 38408-100 Uberlândia-MG, Brazil*

[b]*Instituto de Física, Universidade Federal de Uberlândia, 38408-100 Uberlândia-MG, Brazil*

Table S1. Materials and components employed in assembling the compact liquid-handling robot, with corresponding estimated costs

Part name	Quantity	Price (US$)
ABS filament 1.75 mm / kg	1	13
PETG filament 1.75 mm / kg	0.5	10
Aluminum material / mm	4500	46
Steel rod 8 mm / mm	2000	5
LM8UU linear bearing / u	10	11
GT2 6 mm timing belt / mm	3500	6
GT2 6 mm 20 teeth timing belt pulley / u	2	4
GT2 6 mm idler timing pulley with bearing / u	8	7
Lead screw rods (8 and 6 mm) / mm	600	4
T8 and T6 screw nuts / u	2	2
12 V 3 A power supply / u	1	6
BTT SKR v1.4 motherboard	1	28
Stepper motor NEMA 17 and drivers / u	3	50
Stepper motor NEMA 14 and driver / u	1	14
Stepper Motor Cable 1 meter 4 pins / u	4	4
Mechanical endstop limit switch module / u	4	4
Color sensor / u	1	16
Arduino Uno microcontroller / u	1	10
12 V mini aquarium peristaltic pump / u	2	10
Screws and nuts / u	50	4
Other materials		11
Total cost		ca. USD 270

*e-mail: emrichter@ufu.br

[#]Aline D. Assunção and Diogo M. de Jesus contributed equally to this work.

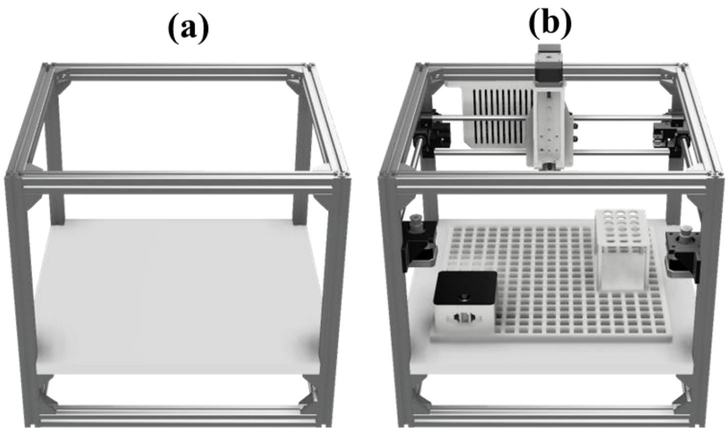

Figure S1. (a) Frame assembly of the liquid handling robot, constructed from 20×20 mm aluminum profiles joined with corner brackets and hammer-head screws. An MDF board supports a modular, reconfigurable platform for flexible device positioning. (b) Fully assembled liquid handling machine.

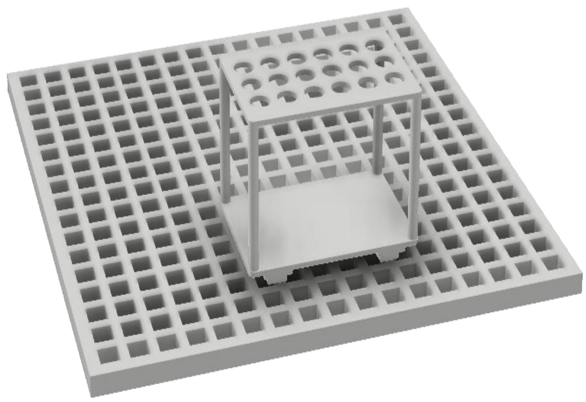

Figure S2. Modular, reconfigurable, grid-shaped platform, customizable with adapters for various devices, including detection cells, sensors, vial racks, beaker holders, and pumps for different applications (modular, practical and customizable).

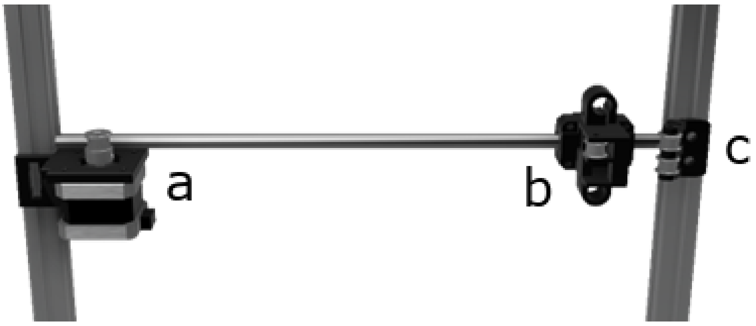

Figure S3. (a) Stepper motor with a pulley for a 6 mm GT2 belt, mounted to the aluminum profile using a PLA-printed part and secured with screws. (b) Carriage featuring a toothed tensioner pulley responsible for motion transmission. (c) PLA-printed part attached to the aluminum profile with smooth tensioning rollers to maintain belt tension. This system is mirrored on the opposite side of the machine.

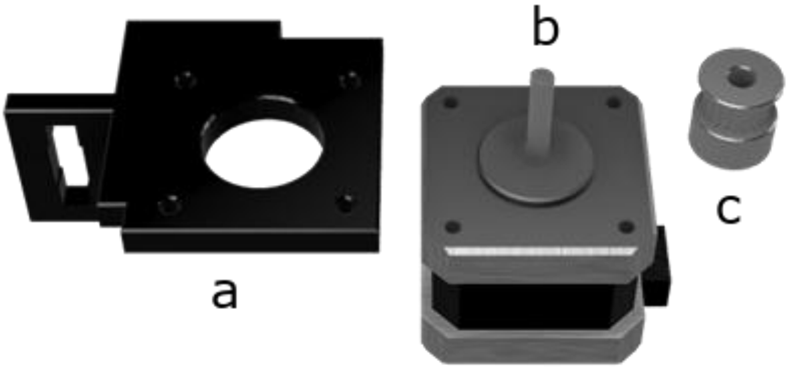

Figure S4. (a) PLA-printed part for stepper motor mounting; (b) NEMA 17 stepper motor; (c) 20-tooth pulley for a 6 mm GT2 belt.

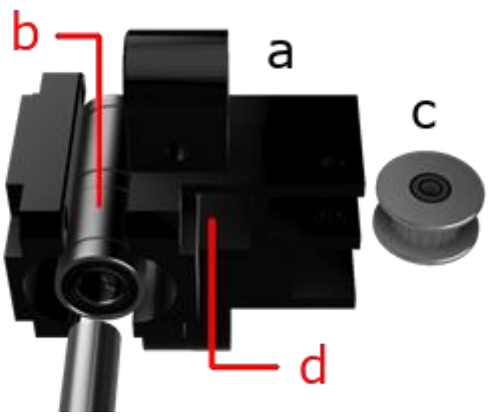

Figure S5. (a) PLA-printed parts joined with screws to secure a (b) LM8LUU linear bearing, which enables sliding along an (c) 8 mm diameter aluminum rod. (d) Toothed tensioner pulley with a ball bearing, mounted on the carriage.

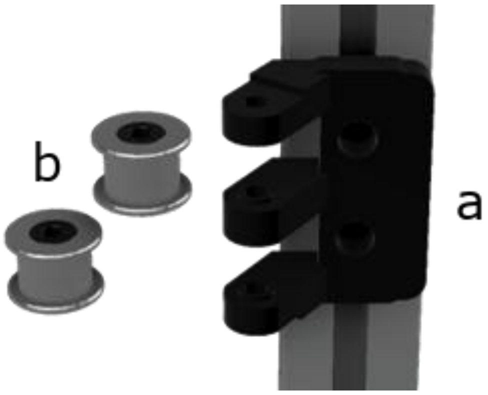

Figure S6. (a) PLA-printed part for mounting (b) smooth tensioning rollers with bearings, designed for a 6 mm GT2 belt.

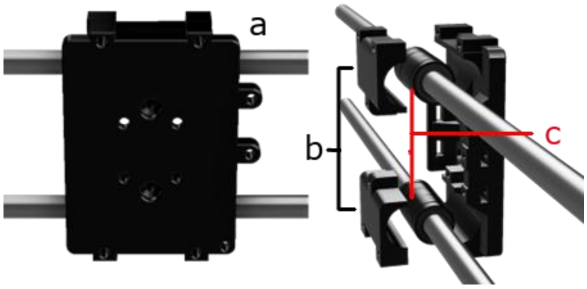

Figure S7. (a) Cartesian XY motion system driven by stepper motors via belt transmission. (b) PLA-printed components for the XY-axis carriage. (c) LM8LUU linear bearings.

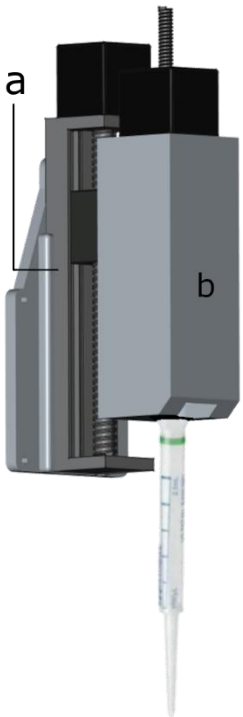

Figure S8. Syringe pump: (a) the Z-axis system consists of a PLA-printed base mounted on the XY-axis carriage, supporting a NEMA 11 stepper motor connected to a threaded rod that drives the lead screw assembly. (b) For liquid aspiration and dispensing, a NEMA 14 stepper motor-with a similar drive mechanism-controls the syringe plunger.

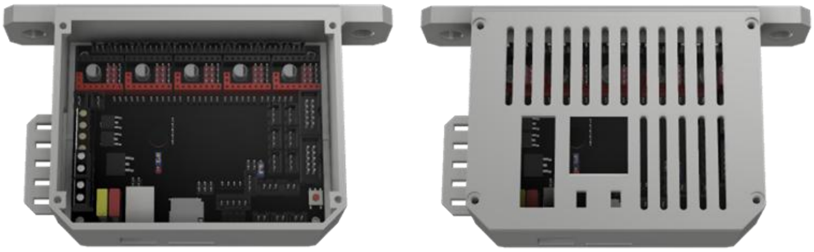

Figure S9. 3D-printed protective housing for the BTT SKR v1.4 motherboard.

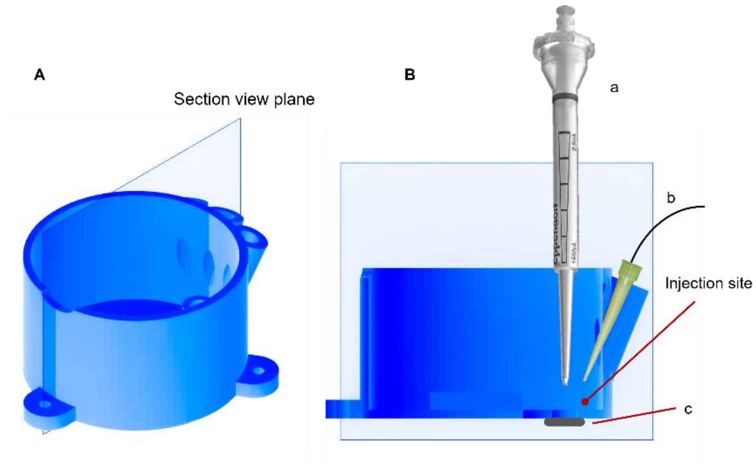

Figure S10. Section view of the 3D-printed electrochemical BIA cell showing the position of the syringe tip close to the electrode surface (a) during the injection process and the inlet (b) for the solution from the mini-aquarium peristaltic pump, which facilitates rapid removal of the injected solution from the sensor surface area. The position of the rubber O-ring (c), which defines the geometric area of the electrode at the base of the BIA cell, is also indicated.

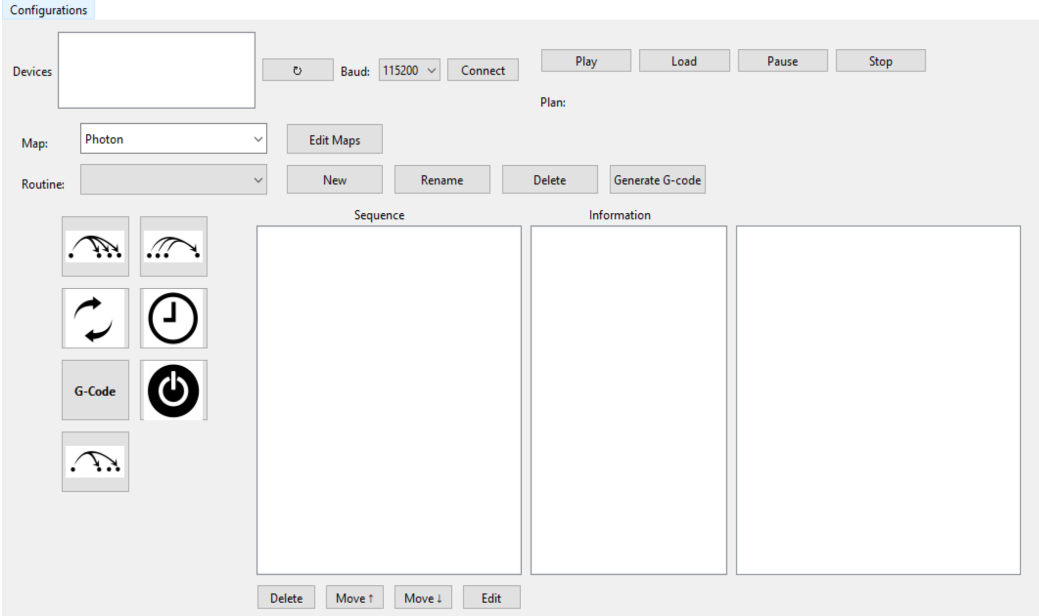

Figure S11. The screenshot displays the main interface of the control software for the automated analysis system. This interface enables a computer to connect to the BTT SKR v1.4 motherboard via serial communication. Once the connection is established, GCODE files containing preconfigured analysis routines can be loaded and sent to the machine. The software provides an intuitive interface for creating new routines, allowing users to insert commands for application, collection, mixing, and pause steps. Additional system functionalities can be accessed through the configuration menu.

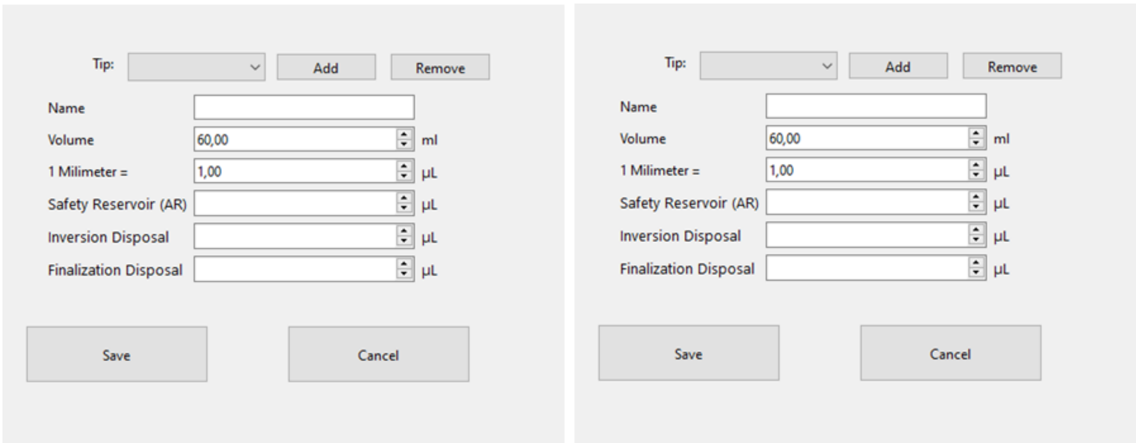

Figure S12. The graphical user interface (GUI) offers precise control over the machine's motion parameters-such as axis speed and acceleration-through numerical input fields and control buttons (a). The tip selection menu enables users to choose the most suitable tip for each application based on its volumetric capacity (b).

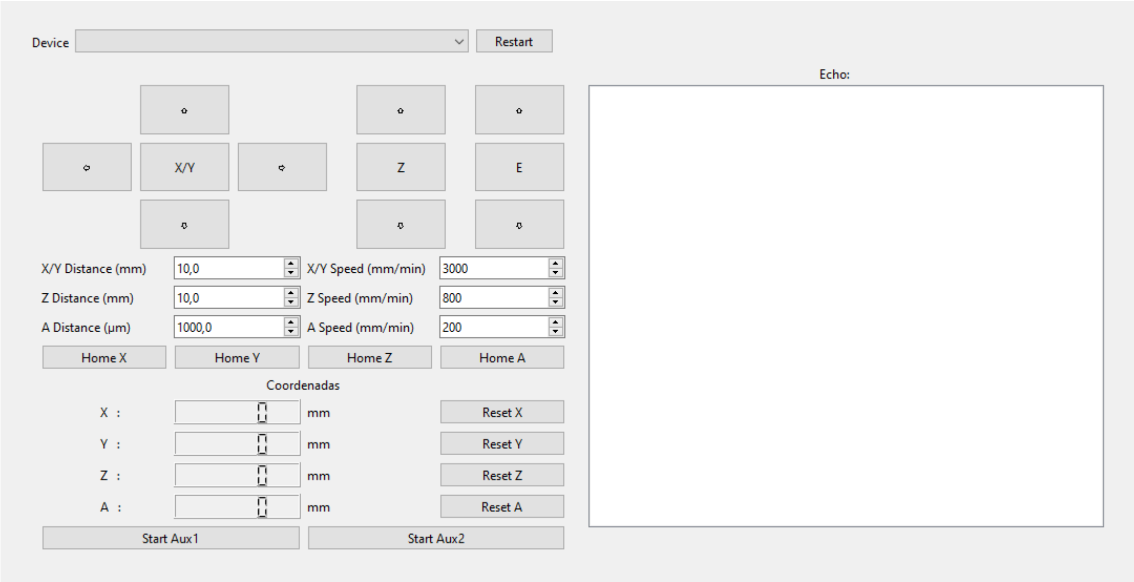

Figure S13. Manual control interface designed for fine-tuning machine movements, enabling precise positioning of components and facilitating testing procedures.

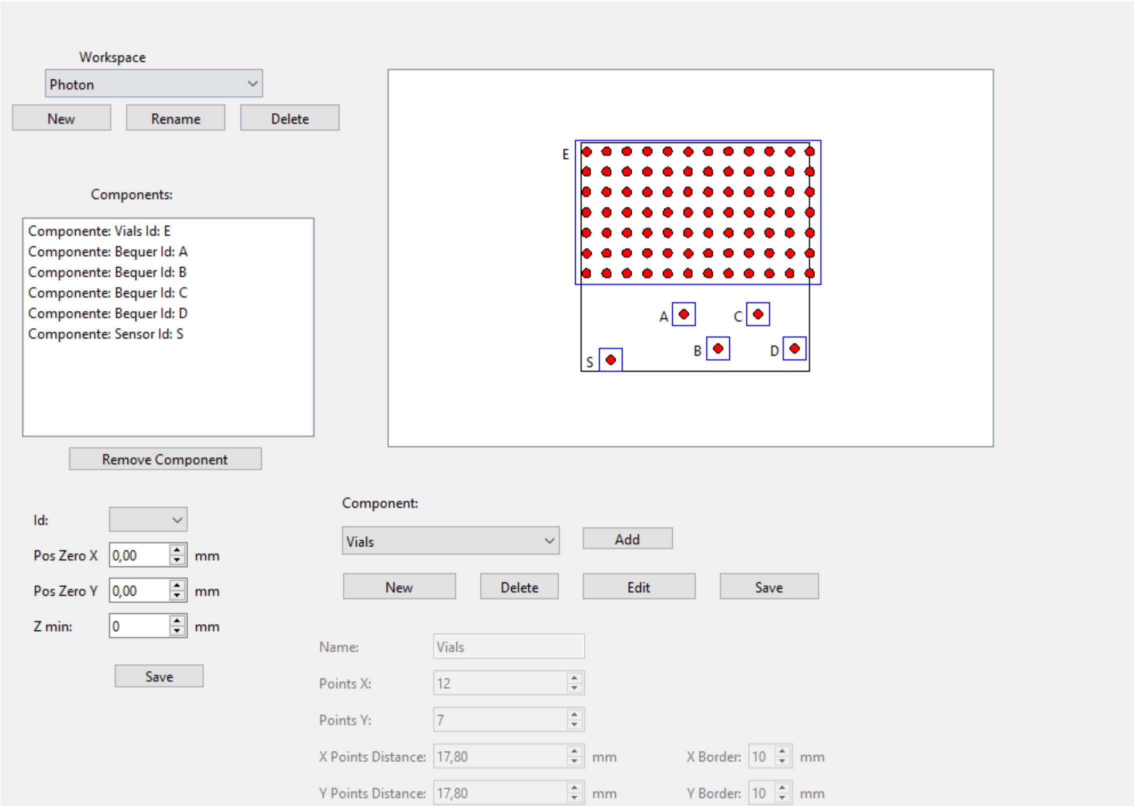

Figure S14. Interface for configuring and saving the Cartesian coordinates of components-such as vials, detection cells or beakers-enabling the development of automated analysis routines.

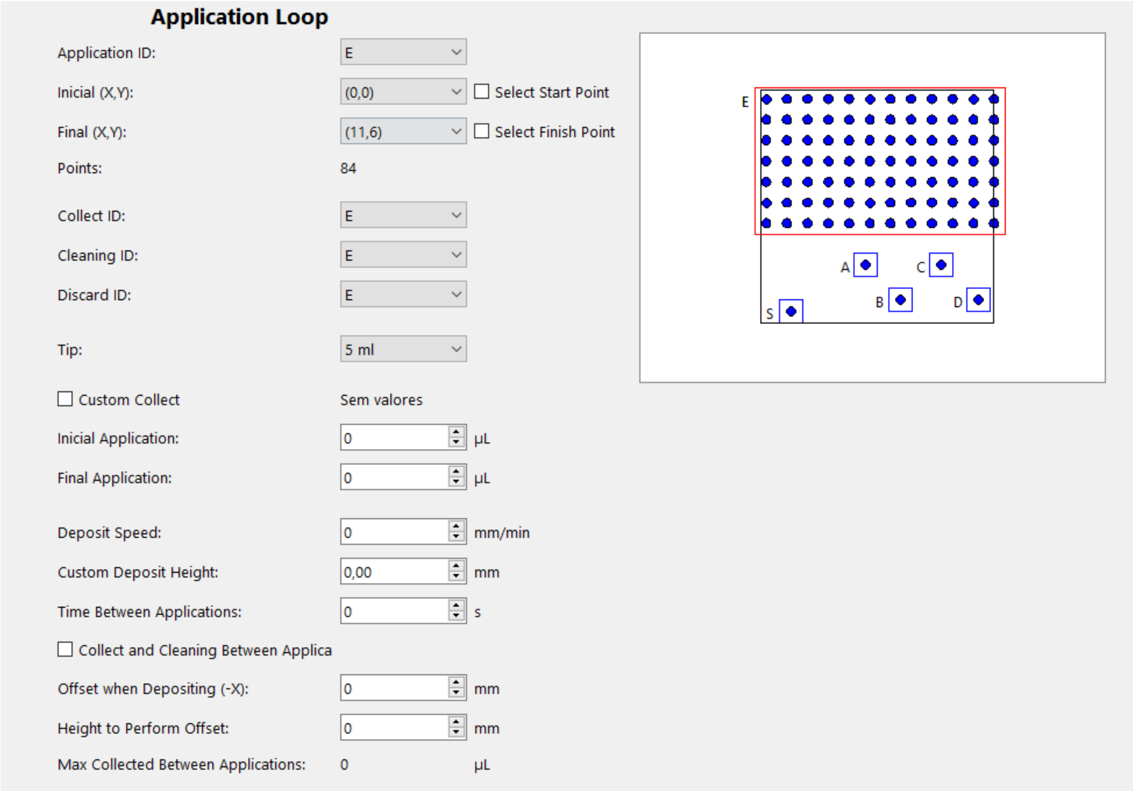

Figure S15. Application cycle configuration interface. This interface allows users to define liquid injection sequences at specific points in the system, based on preconfigured component coordinates.

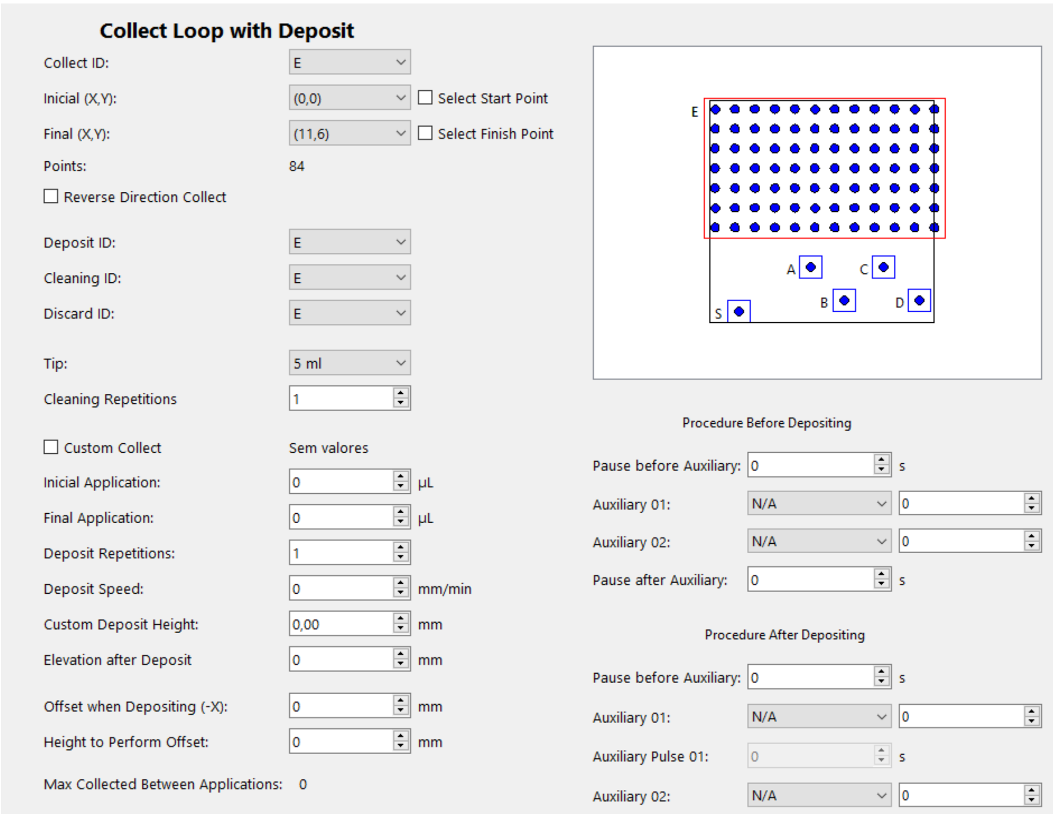

Figure S16. Liquid collection cycle configuration interface. This interface allows users to define liquid aspiration sequences at specific points in the system, based on preconfigured component coordinates.

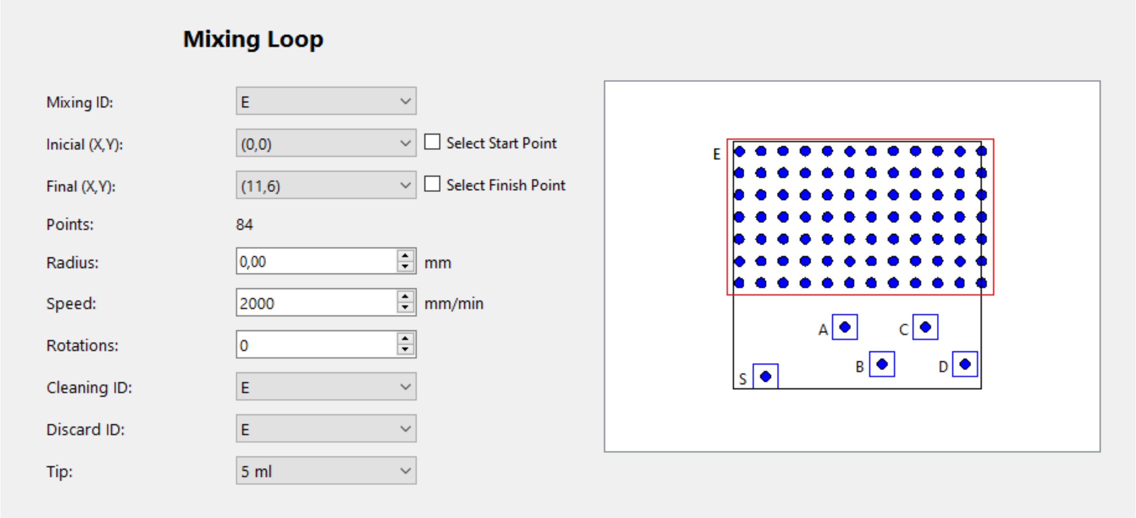

Figure S17. Interface for creating detailed protocols for automated liquid mixing. Through integration with other process cycles, it allows precise definition of the addition sequence, volumes, and mixing conditions such as speed and time.

Table S2. Comparison of the performance between the proposed 3D-printed syringe and a commercial electronic pipette (Combitip® 2.5 mL) for different dispensed volumes (n = 5)

Volume / µL	3D-printed syringe		Commercial pipette	
	Mass / mg	Error / %	Mass / mg	Error / %
50	49.61	–0.8	48.91	–2.1
100	101.72	+1.7	98.43	–1.6
150	152.33	+1.6	148.68	–0.9
200	202.24	+1.1	198.76	–0.6
500	501.01	+0.2	497.90	–0.4
1000	1006.11	+0.6	992.74	–0.7

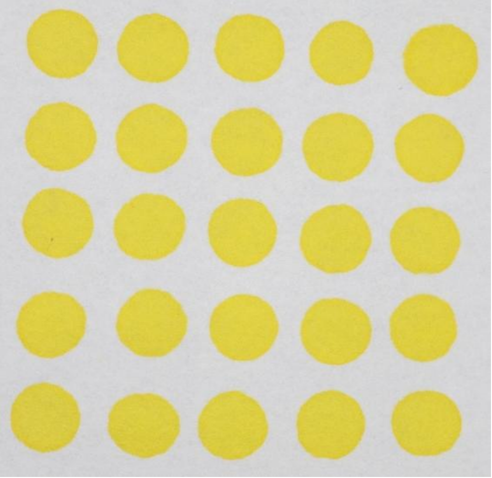

Figure S18. Images showing the spots formed on a sheet of paper after the deposition and drying of 2.0 µL of a yellow dye solution. The RSD of the spot diameter was calculated to be 2.8% (n = 25).

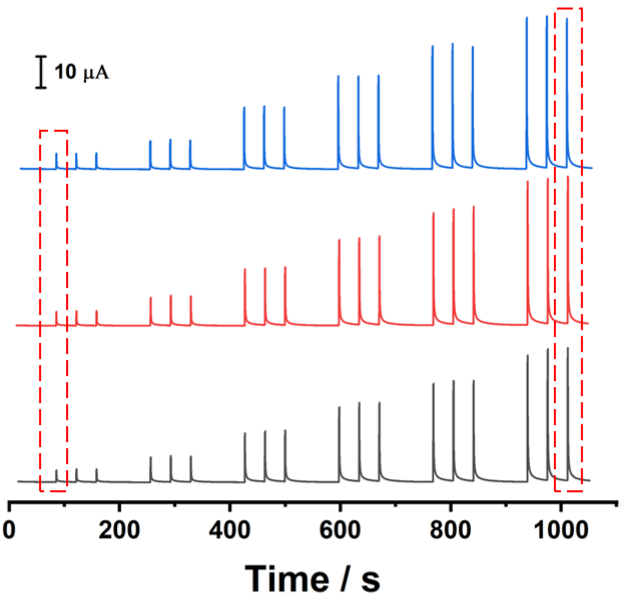

Figure S19. Three independent and sequential BIA-amperograms obtained from successive injections of paracetamol solutions at increasing concentrations (2.5-25.2 mg L^{-1}). Experimental conditions: working electrode - boron-doped diamond; injection volume - 200 µL; dispensing rate - 260 µL s^{-1}; applied potential - +1.0 V *vs.* Ag|AgCl|$KCl_{(sat.)}$; supporting electrolyte - 0.1 mol L^{-1} acetate buffer (pH 4.7).

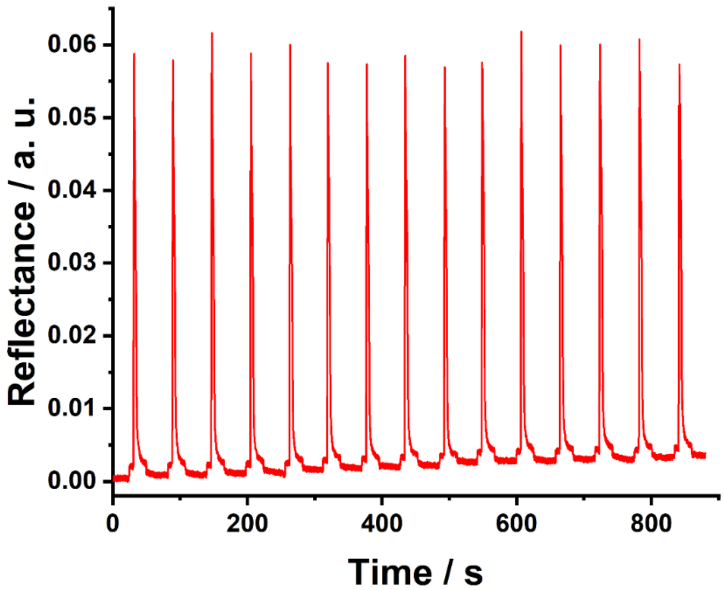

Figure S20. BIAgram (reflectance *vs.* time) obtained from successive injections of fifteen Fe^{III} solutions, all prepared at the same concentration (4.0 mg L^{-1}) using the proposed liquid handling system (RSD = 2.7%; n = 15). Experimental conditions: λ = 480 nm; injection volume = 100 µL; dispensing rate = 150 µL s^{-1}.